ROYAL SOCIETY
OF CHEMISTRY

PAPER

Check for updates

BiOI/melamine foam as an extremely efficient and highly recyclable catalyst for the treatment of continuous flow organic pollutants†

Xinrui Luo,‡[a] Li Tan,‡[b] Liping Wu[a] and Qiuxia Liu [ID] *[a]

The use of nano-catalysts to reduce nitroaromatic compounds is a promising wastewater treatment strategy. In this study, melamine foam (MF) is employed as the substrate, and sheet-like bismuth oxide iodide (BiOI) was grown on its surface through a cross-impregnation process involving $Bi(NO_3)_3$ and KI solution. As a catalyst, bismuth oxide iodide/melamine foam composite (BiOI/MF) exhibits remarkable catalytic activity and excellent durability in the treatment of continuous flow 4-nitrophenol (4-NP) solutions. The loading capacity of BiOI on a $2 \times 2 \times 2$ cm^3 MF substrate is notably low at just 0.13 g, yet it can completely reduce 50 mL 4-NP solution (0.37 mmol L^{-1}) within 32 minutes. After six consecutive cycles, the catalyst maintained a conversion efficiency of over 90%, with the total treatment amount for 4-NP reaching 1.49×10^{-2} mmol. Furthermore, BiOI/MF also exhibited high catalytic reduction activity towards other organic pollutants, such as methylene blue and methyl orange solutions. In this study, we propose an efficient and cost-effective composite catalyst that offers technical guidance for the practical treatment of wastewater and sewage.

1. Introduction

The rapid advancement of urbanization and industrialization has led to the discharge of substantial quantities of organic pollutants, waste gases, and wastewater from the chemical industry, posing significant threats to both environment and human health.[1–3] Among these pollutants, 4-nitrophenol (4-NP)—a critical intermediate in herbicide, pesticide, synthetic dye, and paint production—is extensively utilized in pharmaceutical and textile manufacturing.[4] Notably, 4-NP exhibits acute toxicity, mutagenicity, and tends to accumulate in biological systems.[5,6] Furthermore, its environmental persistence is alarmingly high, with reported half-lives spanning multiple orders of magnitude: photolytic degradation in aqueous media requires 3.1 to 329 h, aqueous photooxidation from 642 to 4.90 $\times 10^4$ h, and atmospheric photooxidation occurs within 14.5 to 145 h.[7,8] In contrast, its reduced derivative, 4-aminophenol (4-AP), demonstrates significantly diminished toxicity,[9] rendering the catalytic conversion of 4-NP to 4-AP not only an environmentally imperative but also a value-added transformation strategy.

Catalytic wastewater treatment technologies face persistent challenges, particularly in terms of catalyst recyclability and cost effectiveness. Noble metal-based catalysts (*e.g.*, Au and Pt) frequently suffer from particle aggregation and separation difficulties, which increase operational costs.[10] Numerous studies have indicated that precious metals (Au, Pd, Ag, Pt) effectively catalyse 4-NP reduction to 4-AP in the presence of sodium borohydride ($NaBH_4$).[11–13] However, their inherent limitations—high expense, irreversible agglomeration during catalysis, and inadequate reusability—often result in secondary pollution of the water body.[14] To overcome these problems, the catalyst was immobilized onto magnetic materials such as Fe_3O_4. For example, Zhou *et al.* synthesized Fe_3O_4@P (MBAAM-Co-MAA)@Ag NPs with magnetic core for 4-NP reduction; however, catalytic activity diminished after merely three cycles.[15] However, the catalytic activity decreased after only 3 cycles. This instability arises from magnetic nanoparticles' tendency to coordinate with water/hydroxyl groups, facilitating interactions with organic/inorganic species and proton/cation adsorption, thereby degrading their structural integrity.[16] Recent advances include Li *et al.*'s ZIF-67-Co-derived Co@NC catalyst, which maintained more than 95% conversion efficiency over 17 reaction cycles, a marked improvement over conventional transition metal nanoparticles.[17] Singh *et al.* further demonstrated the catalytic potential of BiOX (X = Cl, Br, I) semiconductors, where partially reduced Bi^0 species synergistically enhanced the $NaBH_4$-mediated reduction of 4-NP with

[a]*College of Environmental Science and Engineering, China West Normal University, Nanchong 637009, Sichuan, China. E-mail: liuqx10812@163.com*

[b]*Periodical Agency, Editorial Department of Ecology and Environmental Monitoring of Three Gorgee, College of Chemistry and Chemical Engineering, Yangze Normal University, Chongqing 408100, China*

‡ These authors made equal contributions.

BiOX.[18] Nevertheless, BiOX performance declined after 5 cycles due to excessive Bi^0 accumulation impairing reducibility. Critically, when treating large volumes of wastewater, traditional methods involving intermittent filtration, centrifugation, and washing are not only time-consuming and labour-intensive, but also prone to causing substantial material loss.[19] These further compromise the treatment efficiency and economic viability, limiting their practical applicability. Consequently, the development of integrated catalytic membrane systems capable of simultaneously high catalytic efficiency and flux under low-energy consumption and eco-friendly continuous-flow conditions has emerged as a pressing research priority.

Continuous stream treatment offers a continuous and efficient method for contaminant removal, surpassing the efficiency of intermittent treatment methods.[20] It minimizes the risk of secondary pollution by preventing the buildup of pollutants during the treatment process. The automation inherent in continuous flow systems also significantly reduces both labour and operational costs.[21] The most critical component in this system is the membrane catalytic material. Common membrane substrates, including glass fibres, carbon fibres, metallic foams, and organic polymeric networks, exhibit inherent trade-offs. Low-thickness membranes (e.g., carbon fibre cloth) minimize mass transfer resistance but require reduced hydraulic loading to compensate for short reactant residence times.[22,23] Conversely, metallic foam reactors enhance catalytic efficiency through tortuous flow paths but suffer from structural brittleness.[24,25] Melamine foam (MF), a three-dimensional (3D) porous polymer, has gained prominence as an ideal substrate owing to its high specific surface area, cost-effectiveness, and robust stability.[26] Its macro-porous architecture not only mitigates catalyst agglomeration during immersion or in situ growth but also facilitates regeneration and reuse attributes that underscore its potential in membrane catalysis. For instance, Huang et al. grafted polyethyleneimine (PEI) onto melamine foam (MF-PDA) to remove chromium ions ($Cr(VI)$) from water,[27] Li et al. immersed melamine foam in an iron ion solution and carbonized it to produce Fe@MF composites; the block-shaped Fe@MF exhibited a far higher $Cr(VI)$ reduction and adsorption efficiency than nano zero-valent iron particles,[28] and Vo et al. developed a GO-covered MF composite adsorbent by immersing MF in a graphene oxide solution, which demonstrated exceptional adsorption performance for various organic dyes.[29]

To evaluate the catalytic performance under realistic conditions, this study employed a continuous-flow treatment to assess a novel bismuth oxide iodide/melamine foam composite (BiOI/MF) composite catalyst. BiOI was grown in situ on melamine foam via impregnation, which enabled $NaBH_4$-mediated 4-NP reduction at ambient temperatures. The catalyst activity and cyclability were systematically investigated by modulating the pollutant concentration, $NaBH_4$ dosage, and water flow rate to alter the contact time between the target pollutants and the catalyst. Finally, the possibility of applying BiOI/MF to other wastewater treatments is discussed. The results provide design principles for high-efficiency catalytic technologies that are suitable for practical wastewater treatment.

2. Experimental

2.1 Materials

Potassium iodide (KI), sodium borohydride ($NaBH_4$), 4-nitrophenol (4-NP), methylene blue (MB), methyl orange (MO), and ethanol were purchased from Kelon Chemical Reagent Company (Chengdu, China). Bismuth nitrate pentahydrate ($Bi(NO_3)_3 \cdot 5H_2O$) was purchased from Aladdin Co. Ltd (Shanghai, China). Melamine foam (MF) was purchased from the Building Materials Manufacturer (Hangzhou, Zhejiang, China). All chemicals used in this study were of analytical grade and required no further purification.

2.2 The synthesis of BiOI/MF

First, MF was cut into $2 \times 2 \times 2$ cm^3 blocks, washed ultrasonically in deionized water and ethanol for 10 min, and dried at 60 °C for 12 h. Subsequently, 0.10 mol per L $Bi(NO_3)_3$ solution and 0.50 mol per L KI solution were prepared, respectively. The clean MF was immersed in the $Bi(NO_3)_3$ solution for one minute and then soaked in deionized water for 3 to 4 s. Next, it was immersed in KI solution for one minute and then soaked in deionized water for 3–4 s. The above steps were repeated 28 times. Finally, the soaked MF were placed in a clean beaker and baked in an oven at 80 °C for at least eight hours.

2.3 Characterization

An X-ray diffraction (XRD; Shimadzu, Japan) device was used to obtain information about the crystal structures of the synthesized materials. The laser light source used was CuK$^\infty$ ($\lambda = 1.5406$ Å), with a scan range of 5–80. Scanning electron microscopy (SEM, Zeiss, Germany) analysis was performed to reveal the presence of materials in the catalysts and the surface morphology. An energy-dispersive spectrometer (EDS) was used for the elemental analysis. Transmission electron microscopy (TEM) and high-resolution transmission electron microscopy (HRTEM) images were obtained using a Thermo Fisher Talos F200S microscope (Talos F200S, USA). X-ray photoelectron spectroscopy (XPS) was performed using a spectrometer equipped with Al Kα and $h\nu$ (1486.6 eV) under vacuum conditions ($\sim 2 \times 10^{-7}$ Pa) (Thermo Scientific ESCALAB Xi+, USA), and all spectra were standardized using the C 1s peak located at 284.8 eV.

2.4 Experimental

A continuous-flow device was built in this study, as shown in Fig. S1.† The mixed solution of 4-NP and fresh $NaBH_4$ flowed out from the reagent bottle because of the gravitational potential energy difference and atmospheric pressure. The flow rate was adjusted using a regulator to control the mixed solution passing through the BiOI/MF catalyst at a constant speed. The filtrate was then placed in a small beaker. The filtrate was collected every two minutes. The filtrate was detected using a Shimadzu UV2550 spectrophotometer at 25 °C with a spectral range of 200–600 nm and a scanning speed of 1 nm.

A cycling experiment was conducted using the same device. The difference was that in this experiment, the 4-NP solution was not mixed with the fresh $NaBH_4$ solution. Instead, it was directly mixed with the filtrate and continuously catalysed by BiOI/MF.

3. Results and discussion

3.1 Crystal structure and composition analysis

The impregnated foam appeared orange (inset in Fig. 1b), indicating the growth of BiOI on the surface of the MF. The microscopic morphology was observed by SEM, as shown in Fig. 1. The pure MF exhibited a porous network and a smooth surface structure, as shown in Fig. 1a. The BiOI synthesized by the dipping method consists of floral-like structures assembled by ultrathin nanosheets distributed on the MF, and it has a diameter of 5–10 μm (as shown in Fig. 1b and c). EDS and mapping showed that the main elements Bi, O, I, C, and N were evenly distributed, with Bi, I, and O mainly coming from BiOI, and C and N mainly coming from the foam, indicating that BiOI was uniformly distributed on the MF surface (as shown in Fig. 1d–i).

The TEM and HRTEM images (Fig. 2a and b) are consistent with the SEM images, further confirming the flower-like structure of BiOI assembled by nanosheets with a thickness of several nanometres and width ranging from 90 to 110 nm. The lattice spacing of BiOI was observed by HRTEM images to be 0.27 nm (Fig. 2c), which was consistent with the reported BiOI ($d = 0.282$ nm), corresponding to the (110) crystal face of BiOI.[30] And the other lattice spacing of BiOI was 0.91 nm (Fig. 2d), which was consistent with the BiOI ($d = 0.913$ nm), corresponding to the (001) crystal face of BiOI, as evidenced by the large (001) reflection at 9.7° in the XRD.

The crystal structures of the samples were characterized using XRD. As shown in Fig. 3, the characteristic diffraction peaks located at 9.7°, 19.3°, 29.7°, 31.7°, 45.4°, and 55.1° correspond to the (001), (002), (012), (110), (020), and (122) crystal planes of BiOI, respectively. They showed good consistency with the peak positions of the standard tetragonal BiOI
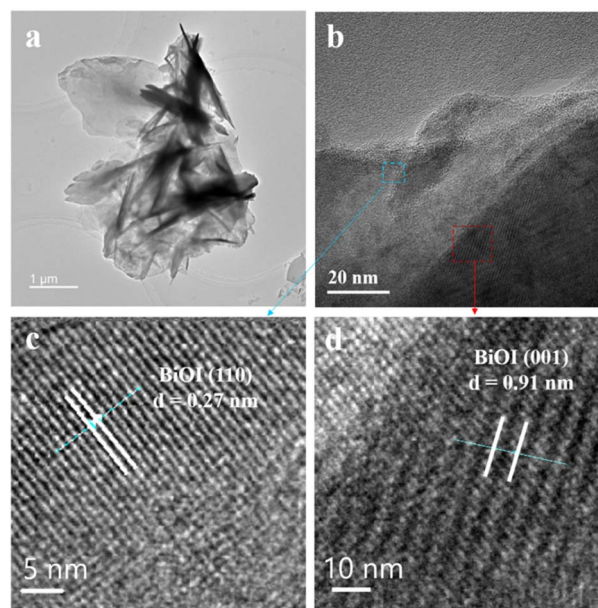

Fig. 2 TEM (a) and HRTEM (b) images of BiOI, ((c) and (d) are taken in (b), (c) is a magnified view of the blue area, and (d) is a magnified view of the red area).

phases (JCPDS no. 73-2062). It can be concluded that BiOI nanosheets mainly expose the (001) and (110) crystal planes, with the (001) plane mainly extending on the (110) crystal plane, as previously reported.[31] The FTIR spectra of MF and BiOI/MF samples are presented in Fig. S2.† For pristine MF, the absorption peak at 3443 cm^{-1} corresponds to N–H stretching vibrations, peaks at 2945 and 2850 cm^{-1} are attributed to C–H stretching vibrations, and the characteristic triazine ring peaks appear at 1530, 1471, 1370, and 805 cm^{-1}, where those at 1530, 1370, and 805 cm^{-1} represent bending vibrations of the ring, while the peak at 1471 cm^{-1} arises from C–N stretching vibrations, the peak at 1620 cm^{-1} is assigned to O–H bending vibrations, peaks at 1200 and 1020 cm^{-1} indicate C–O–C stretching vibrations.[32,33] In BiOI/MF composites, significant attenuation of peaks at 3443, 2920, 2850, 1200, and 1020 cm^{-1}
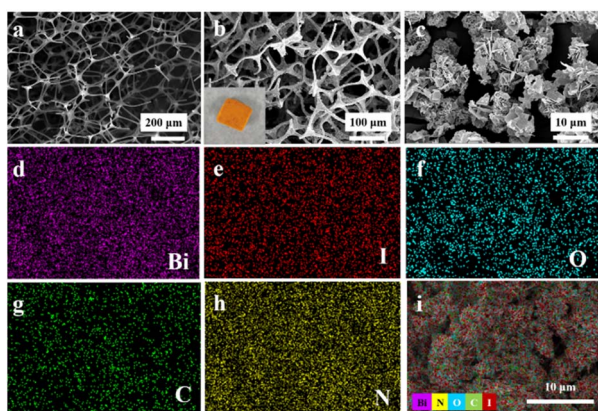

Fig. 1 SEM images of (a) MF and (b and c) BiOI/MF. Elemental mapping images of BiOI/MF, (d) Bi, (e) I, (f) O, (g) C, (h) N and (i) the mixture.
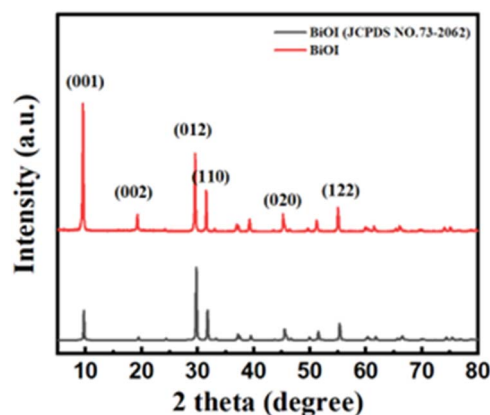

Fig. 3 XRD pattens of BiOI.

are observed, indicating reduced oxygen-containing functional groups and amino groups compared to pristine MF. This confirms chemical interactions between BiOI and MF surface functionalities, resulting in enhanced binding stability.

3.2 Catalytic performance of the samples

To evaluate the catalytic effect of BiOI on the 4-NP reduction process, we followed the steps described in 2.4 in the device shown in Fig. S1.† The mixture of 4-NP and NaBH$_4$ was light yellow, and it had a large absorption peak at 400 nm in the UV-vis absorption spectrum (Fig. 4a), which is due to the formation of 4-nitrophenolate ions. When the mixture passed through BiOI/MF, the colour of the solution immediately changed from light yellow to colourless (Fig. S3†). The UV-vis absorption spectra of the filtrate collected every 2 min showed that the 4-nitrophenolate ion was completely reduced in a short period of time. The results indicate that BiOI/MF had excellent conversion efficiencies for the continuous flow of 4-NP.

In contrast, controlled experiments have confirmed that BiOI/MF has a good removal effect on 4-NP during catalytic reduction by NaBH$_4$. BiOI powder was directly put into a mixed solution of 4-NP and NaBH$_4$ (purple in Fig. 4b and S4†), the powder was quickly reduced into black, and 50 mL of 4-NP completely reduced in 1 min, but the powder was not easy to collect, which was not conducive to its recycling in actual application. Without BiOI/MF (red in Fig. 4b) and only MF without BiOI (blue in Fig. 4b), the concentration of the 4-NP filtrate was barely reduced. However, when BiOI powder was coated on the MF surface (orange in Fig. 4b) or the BiOI/MF block was immersed in a mixture of 4-NP and NaBH$_4$ (green in Fig. 4b and S5†), the concentration of the 4-NP filtrate decreased significantly, with removal efficiencies of over 90%.

By controlling the liquid flow rate, pollutant concentration, and NaBH$_4$ concentration, the contact time between 4-NP and the catalyst could be adjusted to study the activity of the catalyst from multiple perspectives. First, while keeping the ratio of 4-NP to NaBH$_4$ constant, by changing the flow rate of continuous flow, it is observed that both increasing or decreasing the flow rate will lead to a decrease in the catalytic efficiency (22 days per min > 15 days per min > 28 days per min ≈ 35 days per min), and t2e optimal flow rate is 22 days per min (as indicated in Fig. 4c). As the concentration of 4-NP rises from 4.95×10^{-5} mol L^{-1} to 3.70×10^{-4} mol L^{-1}, the catalytic degradation rate of 4-NP is decreased. (as shown in Fig. 4d). When the concentration of NaBH$_4$ was reduced (Fig. 4e), the catalytic degradation effect was slightly weakened. This indicates that the more fully 4-NP contacts the catalyst, the higher is the reduction efficiency. In the above catalytic process, a significant colour change was observed. It was speculated that this was caused by the reduction of the BiOI catalyst to Bi^0 by NaBH$_4$.

3.3 The important role of Bi^0 in catalytic reduction

To confirm this hypothesis, BiOI/MF was soaked in the same concentration of NaBH$_4$ solution for ten minutes until the foam turned black (Fig. S6†). Subsequently, a mixed solution of 4-NP and NaBH$_4$ was passed continuously through the catalyst foam. The removal effect of the black catalyst on 4-NP is comparable to that of the yellow catalyst (Fig. 4f). The powder on the black foam was subjected to ultrasonic oscillation and characterized by XRD and TEM (Fig. S7 and S8†). It was discovered that the crystal structure of the catalyst changed significantly, with the
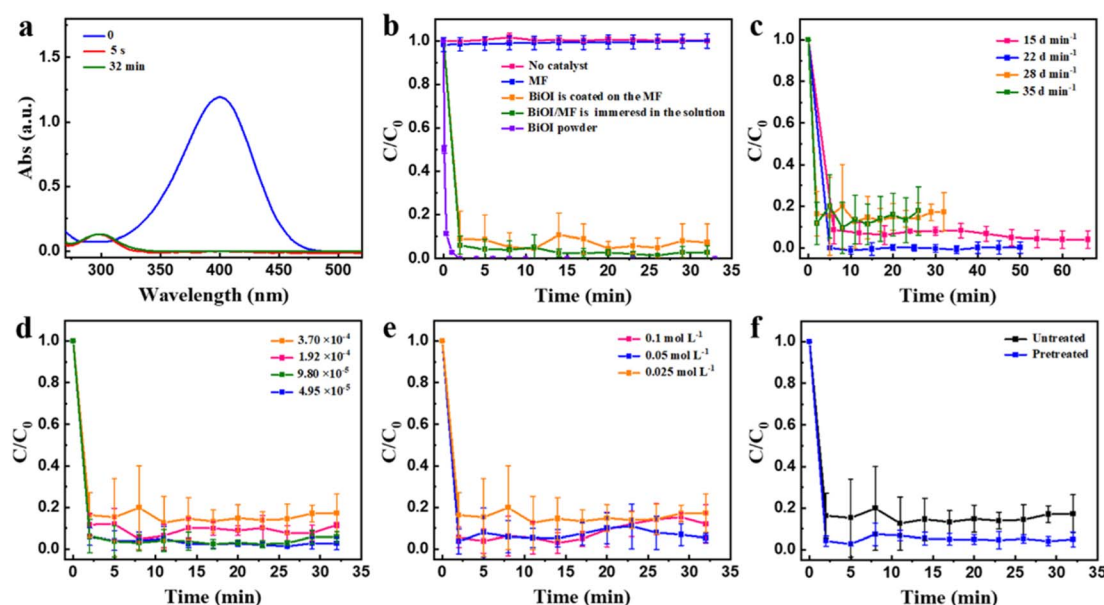

Fig. 4 (a) UV–vis absorption spectra of 4-NP for continuous catalytic reduction by BiOI/MF (4-NP concentration: 3.70×10^{-4} mol per L, NaBH$_4$ concentration: 0.1 mol L^{-1}, flow rate: 28 days per min); (b) control groups (red line of no BiOI/MF, blue line of no BiOI, orange line of directly coated with BiOI powder on MF surface, green line of BiOI/MF is directly immersed in 4-NP and NaBH$_4$ mixed solution and purple line of BiOI powder); (c) different flow rates; (d) different concentrations of 4-NP; (e) different concentrations of NaBH$_4$; and (f) the same concentration of NaBH$_4$ for pretreated/untreated BiOI/MF.

appearance of the characteristic diffraction peaks of Bi^0. The peaks at 27.2°, 38.1°, and 39.8° can be indexed to the (012), (104), and (110) crystal planes of rhombohedral Bi (JCPDS NO. 44-1246) (Fig. S7†). However, the morphology of the catalyst did not change significantly except that in addition to the lattice fringes of BiOI (d = 0.21 nm, (113) crystal plane), the lattice fringes of elemental Bi (d = 0.34 nm, (012) crystal plane) were also found on the catalyst (Fig. S8†).

The valence states of Bi in the catalyst before and after the reaction were also compared using XPS analysis. As shown in Fig. 5, the Bi 4f spectra of BiOI/MF before and after the reaction were deconvoluted into four peaks. The peaks observed at approximately 156.64 and 161.96 eV, which may be attributed to Bi^0. The other peaks located at approximately 158.77 and 164.07 eV, are related to the oxidation state of Bi^{3+}. The peaks of O 1s at 532.41 eV and 531.20 eV were significantly enhanced and were attributed to surface adsorption of O_{water} and O_{ads}. However, there was no significant change in I 3d. The XPS results confirmed that Bi^0 was formed on the surface of BiOI during the catalytic reduction of 4-NP by $NaBH_4$, indicating that $NaBH_4$ partially reduced BiOI to Bi^0. According to the literature, Bi^0 exhibits metalloid properties and can be used as a conductive medium to effectively promote the interfacial transfer of electrons.[34,35] Therefore, Bi^0–BiOI synergistically catalyses the efficient hydrogenation reduction of 4-NP.

3.4 BiOI/MF application potential

To assess the practical application potential of BiOI/MF in the treatment of continuous-flow organic pollutants, we designed a cycle experiment that is like practical applications. Once 4-NP was introduced into the filter solution, $NaBH_4$ was recycled repeatedly. It was discovered that the removal efficiency of 4-NP
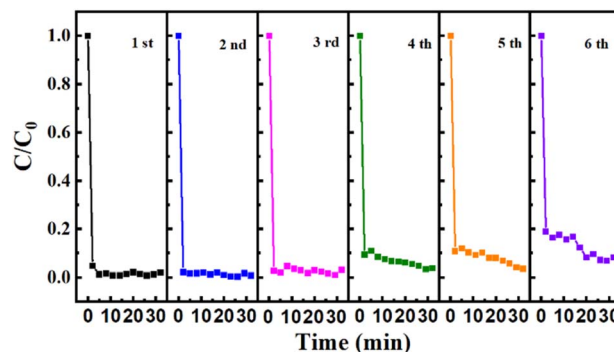

Fig. 6 Reusability test of the BiOI/MF for the catalytic reduction of 4-NP.

remained within the range of 90–98% over six cycles spanning 198 min (as shown in Fig. 6). Furthermore, the total processing capacity of 4-NP amounted to 1.49×10^{-2} mmol, which indicates the remarkable efficacy of BiOI/MF in treating the continuous flow of 4-NP. Compared with previously reported results, the activity of BiOI/MF has reduced efficiency and cyclic effect comparable to those of most reported noble catalysts[36,37] (Table S1†).

To test the versatility of BiOI/MF for organic contaminant removal, we further extended the system to catalyze the reduction of methylene blue (MB) and methyl orange (MO) solutions. Fig. 7a and b present the variations in the ultraviolet-visible absorption spectra of continuous-flow MB and MO in the presence of $NaBH_4$ catalyzed by BiOI/MF. After 2 min of reaction, the absorbance at the maximum wavelength nearly vanished; correspondingly, the colors of the MB and MO solutions disappeared rapidly (Fig. 7c and d). By contrast, control experiments using MF alone exhibited minimal removal efficiencies
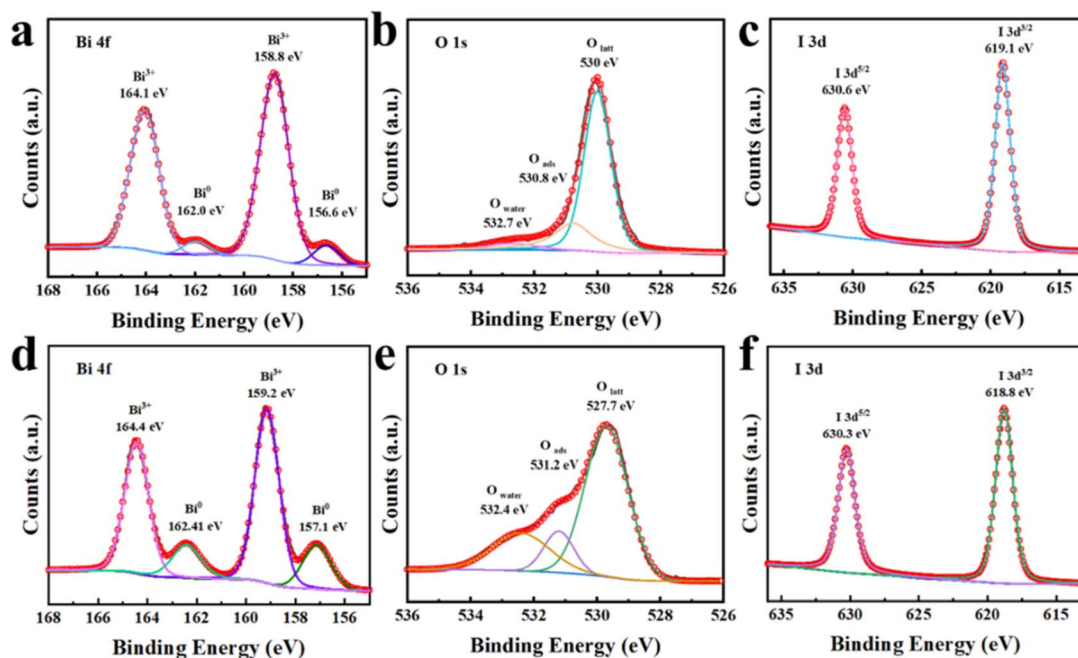

Fig. 5 XPS of BiOI before (a–c) and after (d–f) reaction: Bi 4f (a and d), O 1s (b and e) and I 3d (c and f).
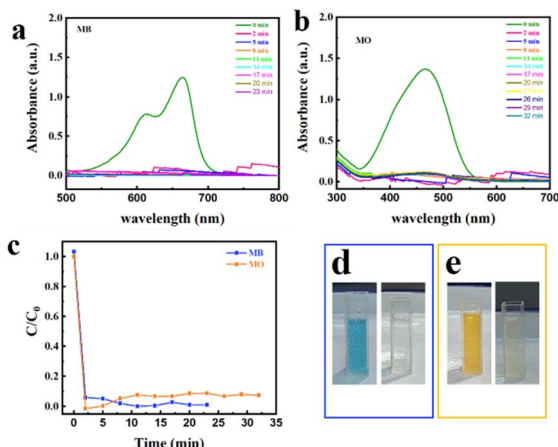
Fig. 7 UV-vis absorption spectra of (a) methylene blue (MB) and (b) methyl orange (MO) for continuous catalytic reduction by BiOI/MF; (c) reduction catalytic efficiency of methylene blue and methyl orange over time; colour contrast of (d) methylene blue and (e) methyl orange before and after reaction.

for MB and MO ($\sim$1.4%) (Fig. S9†), confirming negligible adsorption contributions. These results demonstrate BiOI/MF's exceptional catalytic activity toward organic pollutant degradation (MB and MO), indicating that dye removal occurs primarily through catalytic degradation pathways.

4. Conclusions

In this study, BiOI was grown *in situ* on melamine foams through impregnation, and it catalysed the reduction of 4-NP and other organic contaminants at ambient temperatures. The characterization results indicated the presence of a trace amount of Bi metal in BiOI, which could promote electron transfer on the surface of the material and enhance its catalytic activity. The activity and cycle stability of the catalysts were investigated from multiple perspectives through a cycling experiment. Herin, 50 mL 4-NP (3.70×10^{-4} mol L^{-1}) is completely removed within 5 minutes with flow rate of 35 days per min. BiOI/MF exhibited excellent catalytic removal efficacy at different pollutant concentrations, different NaBH$_4$ concentrations, adjustable water flow speeds, and altered contact time between the target pollutants and the catalyst. Moreover, BiOI/MF exhibited excellent catalytic removal efficacy for methylene blue and methyl orange. The results provide guidance for the design of an efficient catalytic technology suitable for practical wastewater treatment.

Data availability

The authors confirm that the data supporting the findings of this study are available within the article and its ESI.†

Author contributions

Qiuxia Liu: formal analysis, funding acquisition, project administration, writing – review & editing. Xinrui Luo: investigation, data curation, methodology, software. Li Tan: funding acquisition, writing – original draft. Liping Wu: investigation, data curation.

Conflicts of interest

The authors declare no conflicts of interest exist.

Acknowledgements

Notes and references

1 X. Wang, L. Xin, X. Li, L. Qin, T. Zhang and S.-Z. Kang, *Inorg. Chem. Commun.*, 2023, **153**, 110880.

2 B. Weng, M. Zhang, Y. Lin, J. Yang, J. Lv, N. Han, J. Xie, H. Jia, B.-L. Su, M. Roeffaers, J. Hofkens, Y. Zhu, S. Wang, W. Choi and Y.-M. Zheng, *Nat. Rev. Clean Technol.*, 2025, **1**, 201–215.

3 J. Lei, H. Yang, B. Weng, Y.-M. Zheng, S. Chen, P. W. Menezes and S. Meng, *Adv. Energy Mater.*, 2025, 2500950.

4 Q. Liu, Y. Wang, M. Wen, Y. Guo, Y. Wei, G. Li and T. An, *Environ. Sci.: Nano*, 2022, **9**, 4162–4176.

5 U. Ensenbach and R. Nagel, *Comp. Biochem. Physiol. C Comp. Pharmacol.*, 1991, **100**, 49–53.

6 E. Tugba Saka and K. Tekintas, *J. Mol. Struct.*, 2020, **1215**, 128189.

7 T. Braman, L. Dolvin, C. Thrasher, H. Yu, E. Q. Walhout and R. E. O'Brien, *Environ. Sci. Technol. Lett.*, 2020, **7**, 248–253.

8 A. B. Dalton and S. A. Nizkorodov, *Environ. Sci. Technol.*, 2021, **55**, 14586–14594.

9 H. Zhao, X. Pang, Y. Huang, C. Ma, H. Bai and W. Fan, *Inorg. Chem.*, 2022, **61**, 19806–19816.

10 H. Huang, J. Zhao, H. Guo, B. Weng, H. Zhang, R. A. Saha, M. Zhang, F. Lai, Y. Zhou, R.-Z. Juan, P.-C. Chen, S. Wang, J. A. Steele, F. Zhong, T. Liu, J. Hofkens, Y.-M. Zheng, J. Long and M. B. J. Roeffaers, *Adv. Mater.*, 2024, **36**, 2313209.

11 W. Sun, L. Zang, X. Zhang, C. Zhang, Z. Zhang, X. Wang, G. Zhang, F. Wang and T. Zhou, *New J. Chem.*, 2024, **48**, 4548–4557.

12 Y. Chen, S.-C. Wu, J.-J. Han, X. Yan, X.-J. Guo and W.-Z. Lang, *J. Membr. Sci.*, 2023, **687**, 122098.

13 S. Oh, H. Jun, S. Lee and M. Oh, *Inorg. Chem.*, 2022, **61**, 16501–16508.

14 E. Park, J. Jack, Y. Hu, S. Wan, S. Huang, Y. Jin, P.-C. Maness, S. Yazdi, Z. Ren and W. Zhang, *Nanoscale*, 2020, **12**, 2596–2602.

15 W. Zhou, Y. Zhou, Y. Liang, X. Feng and H. Zhou, *RSC Adv.*, 2015, **5**, 50505–50511.

16 M. Bano, D. Ahirwar, M. Thomas, G. A. Naikoo, M. U.-D. Sheikh and F. Khan, *New J. Chem.*, 2016, **40**, 6787–6795.

17 X. Li, C. Zeng, J. Jiang and L. Ai, *J. Mater. Chem. A*, 2016, **4**, 7476–7482.

18 D. Singh and P. Poddar, *New J. Chem.*, 2024, **48**, 9840–9855.

19 Z.-C. Xiong, Y.-J. Zhu, Z.-Y. Wang, Y.-Q. Chen and H.-P. Yu, *Adv. Funct. Mater.*, 2022, **32**, 2106978.

20 S. Babanova, J. Jones, S. Phadke, M. Lu, C. Angulo, J. Garcia, K. Carpenter, R. Cortese, S. Chen, T. Phan and O. Bretschger, *Water Environ. Res.*, 2020, **92**, 60–72.

21 J. Abdi and H. Abedini, *Chem. Eng. J.*, 2020, **400**, 125862.

22 A. Shahzeydi, M. Ghiaci, L. Jameie and M. Panjepour, *Appl. Surf. Sci.*, 2019, **485**, 194–203.

23 Y. Zhu, M. T. Chen, Y. Feng, Q. Ai, Y. Liu, Y. Yan, Q. Li and J. Lou, *Small Struct.*, 2025, **6**, 2400389.

24 X. Liao, X. Wang, L. Zheng, Y. Hu, A. Wu and G. Li, *Process Saf. Environ. Prot.*, 2024, **182**, 1227–1236.

25 T. Du, Z. Zheng, L. Ma, Y. Xu, X. Liao, B. Yuan, M.-L. Fu and Y.-b. Hu, *J. Environ. Chem. Eng.*, 2025, **13**, 116623.

26 J. Pinto, S. Barroso-Solares, D. Magrì, F. Palazon, S. Lauciello, A. Athanassiou and D. Fragouli, *polymers*, 2020, **12**, 934.

27 T. Huang, S. Cao, D. Luo, N. Zhang, Y.-z. Lei and Y. Wang, *Chemosphere*, 2022, **287**, 132054.

28 Q. Li, M. Liu, X. Qiu, X. Liu, M. F. Dapaah, Q. Niu and L. Cheng, *Nanomaterials*, 2022, **12**, 1866.

29 T. S. Vo and T. T. B. C. Vo, *Prog. Nat. Sci. Mater. Int.*, 2022, **32**, 296–303.

30 K. M. Alam, P. Kumar, P. Kar, A. Goswami, U. K. Thakur, S. Zeng, E. Vahidzadeh, K. Cui and K. Shankar, *Nanotechnology*, 2020, **31**, 084001.

31 T. Feeney, G. Aygur, T. Nguyen, S. Farooq, J. Mendes, H. Tuohey, D. E. Gómez, E. Della Gaspera and J. van Embden, *Nanotechnology*, 2023, **34**, 305404.

32 X. Wang, Q. Wang, X. Cheng, X. Chen and M. Bai, *Materials*, 2023, **16**, 7067.

33 K. Hu, H. Lyu, H. Duan, Z. Hu and B. Shen, *J. Hazard. Mater.*, 2024, **465**, 133489.

34 C. Zhang, W. Chen, D. Hu, H. Xie, Y. Song, B. Luo, Y. Fang, W. Gao and Z. Zhong, *Green Energy Environ.*, 2022, **7**, 680–690.

35 C. Zhou, C. Jiang, R. Wang, J. Chen and G. Wang, *Ind. Eng. Chem. Res.*, 2020, **59**, 8183–8194.

36 Y. Li, H. Xu and G. Zhang, *J. Environ. Chem. Eng.*, 2022, **10**, 108677.

37 K. Shanmugaraj, R. V. Mangalaraja, V. Manikandan, C. H. Campos, S. Packiaraj, R. Aepuru, J. Noé Díaz de León, M. Sathish and K. S. Song, *J. Environ. Chem. Eng.*, 2024, **12**, 112942.